PHYSICAL REVIEW C **79**, 011302(R) (2009)

Persistent decoupling of valence neutrons toward the dripline: Study of ^{20}C by γ spectroscopy

Z. Elekes,[1] Zs. Dombrádi,[1] T. Aiba,[2] N. Aoi,[3] H. Baba,[3] D. Bemmerer,[4] B. A. Brown,[5] T. Furumoto,[6] Zs. Fülöp,[1] N. Iwasa,[7] Á. Kiss,[8] T. Kobayashi,[7] Y. Kondo,[9] T. Motobayashi,[3] T. Nakabayashi,[9] T. Nannichi,[9] Y. Sakuragi,[3,6] H. Sakurai,[3] D. Sohler,[1] M. Takashina,[10] S. Takeuchi,[3] K. Tanaka,[3] Y. Togano,[11] K. Yamada,[3] M. Yamaguchi,[3] and K. Yoneda[3]

[1]*Institute of Nuclear Research of the Hungarian Academy of Sciences, P. O. Box 51, H-4001 Debrecen, Hungary*

[2]*Niigata University, Niigata 950-2181, Japan*

[3]*Institute of Physical and Chemical Research (RIKEN), 2-1 Hirosawa, Wako, Saitama 351-0198, Japan*

[4]*Forschungszentrum Dresden-Rossendorf, Bautzner Landstrasse 128, 01328 Dresden (Rossendorf), Germany*

[5]*National Superconducting Cyclotron Laboratory and Department of Physics and Astronomy, Michigan State University East Lansing, Michigan 48824-1321, USA*

[6]*Department of Physics, Osaka City University, Osaka 558-8585, Japan*

[7]*Tohoku University, Sendai, Miyagi 9808578, Japan*

[8]*Eötvös Loránd University, 1117 Budapest, Pázmány Péter sétány 1/A, Hungary*

[9]*Tokyo Institute of Technology, 2-12-1 Oh-Okayama, Megro, Tokyo 152-8551, Japan*

[10]*Research Center for Nuclear Physics (RCNP), Osaka University, Osaka 567-0047, Japan*

[11]*Rikkyo University, 3 Nishi-Ikebukuro, Toshima, Tokyo 171, Japan*

(Received 23 July 2008; published 29 January 2009)

The very neutron-rich nucleus ^{20}C has been investigated by inelastic scattering on ^{208}Pb and liquid hydrogen targets. Through distorted wave analysis, the reduced electric quadrupole transition probability $B(E2; 0^+_{\text{g.s.}} \rightarrow 2^+_1) < 18.4$ (stat) e^2 fm^4 and the neutron transition probability $M_n^2 = 292 \pm 52$ (stat) fm^4 have been derived. A simple shell model calculation has shown a need for a factor of about 0.4 decrease of the normal polarization charges to elucidate the results. This is interpreted as a decoupling of the valence neutrons from the nuclear core in carbon isotopes heavier than ^{14}C.

DOI: 10.1103/PhysRevC.79.011302 PACS number(s): 23.20.Js, 25.60.−t, 27.30.+t, 29.30.Kv

Nuclei close to the dripline are especially important in nuclear structure studies and have been extensively investigated because their properties significantly differ from those of the stable isotopes. One of the most exotic phenomena is the neutron halo, which is formed by the extremely weakly bound neutrons that decouple from the nuclear core [1] leading to the appearance at low excitation energies of a soft dipole mode [2]. A few years ago, the decoupling of more strongly bound neutrons in heavy carbon and boron isotopes was reported [3–6], which was observed as a reduction of the quadrupole polarization charge of the neutrons. This suppression of the polarization charge was associated with the extended distribution of the valence neutrons [7–9] detected in reaction cross section measurements [10]. This might also be accompanied with the change of the structure of the giant quadrupole resonance in neutron-rich nuclei [7,8,11].

Recently, the lifetime of the 2^+_1 state in ^{16}C has been remeasured, and the decoupling phenomenon has been questioned [12]. In the present paper, we report on a study of the neutron and proton transition strengths and polarization charges investigated by inelastic scattering processes in the heavy carbon isotope ^{20}C, lying next to ^{19}C which shows halo characteristics in its ground state [13–15]. Our aim is to provide evidence that the decoupling phenomenon exists in the carbon isotopic chain.

The experiment was carried out at RIKEN Nishina Center, where a ^{40}Ar primary beam of 63 MeV energy and 700 pnA intensity was delivered to a 0.2 mm thick ^{181}Ta production target in which various isotopes were created via the fragmentation process. The RIKEN isotope separator (RIPS) [16] analyzed the momentum and mass of the ejectiles. For purifying purposes, an aluminum wedge degrader of 221 mg/cm^2 thickness was put at the momentum dispersive focal plane (F1). The fragment separator was operated at its full 6% momentum acceptance in order to achieve a ^{20}C beam intensity as high as around 10 particles per second (pps). The resultant cocktail beam also included ^{17}B, ^{19}C, ^{21}N, and ^{22}N isotopes with a total intensity of 100 pps. The identification of these incident beam constituents could be performed on an event-by-event basis using energy loss (ΔE), time-of-flight (TOF), and magnetic rigidity ($B\rho$) information [17]; however, only TOF and ΔE were used in the real runs since the parallel plate avalanche counter (PPAC) at F1 for position measurements and $B\rho$ determination had only 60% efficiency. The ΔE-TOF-$B\rho$ method provided perfect separation of the different isotopes, while the latter one made a complete Z discrimination of the components possible, which was sufficient for our intentions. The TOF was measured between two plastic scintillators of 0.3 mm thickness placed at the first and second focal planes (F2 and F3), while a Si detector of 0.1 mm thickness at F2 provided the ΔE value. With PPACs monitoring the cocktail beam at F2 and F3, it was transmitted to the secondary targets of ^{208}Pb and liquid hydrogen, which had thicknesses of 1445 and 190 mg/cm^2, respectively. The reaction occurred at 37.6 MeV/nucleon mean energy (middle of the target) in the Pb run and 41.4 MeV/nucleon in the ^{1}H run. The scattered particles were detected and identified by the ΔE-TOF-E method. The ΔE was determined by a 1 mm thick plastic scintillator, which also provided the start signal for TOF, placed 80 cm downstream of the target. The

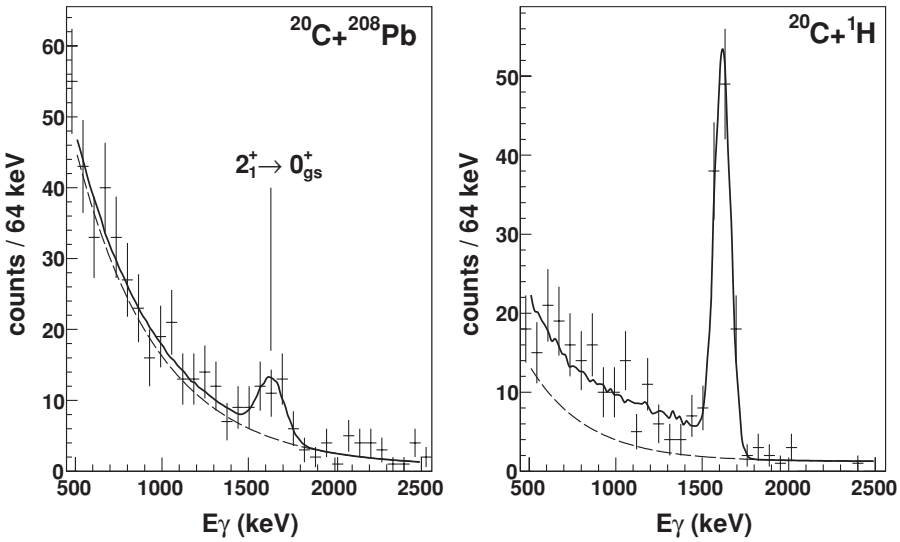

FIG. 1. Doppler-corrected spectra of γ rays emerging from ^{20}C+^{208}Pb and ^{20}C+^{1}H reactions. The solid line is the final fit including the spectrum curves from GEANT4 simulation; additional smooth polynomial backgrounds are plotted as separate dotted lines.

beamlike ions came to a halt at an array of plastic detectors measuring the total energy of the isotopes and giving the TOF stop signal, situated 4.3 m downstream of the target. The array consisted of 16 bars of 60 mm thickness with a total area of 1×1 mm^2. The angular acceptance was 6.5° in the laboratory frame, which granted almost 100% coverage of the cross section. A stack of 160 NaI(Tl) crystals called DALI2 [18] surrounded the target to detect the deexcitation γ rays emitted by the inelastically scattered nuclei. The separation of the scattered isotopes leaving the target was crucial, since lower-mass carbon isotopes were produced by neutron knockout reactions in the liquid hydrogen target. (For the Pb target, this process was negligible.) The Z identification was complete by using the ΔE and TOF information, while the TOF-E two-dimensional spectrum was linearized by a polynomial function, which resulted in a variable called mass number. The segregation in this variable was fairly good, although there was some leakage between the adjacent isotopes. However, the even mass isotopes were completely distinct, and the $2_1^+ \rightarrow 0_{\text{g.s.}}^+$ transition in ^{20}C was free of this effect.

The resulting Doppler-corrected γ-ray spectra for ^{20}C can be seen in Fig. 1. Single peaks were observed at 1631(37) and 1614(11) keV in the left and right panels, respectively, by fitting the spectra with Gaussian functions and smooth polynomial backgrounds. These peaks correspond to a transition between the first 2^+ excited and the ground state of ^{20}C, and their energies are in good agreement with the previously determined value of 1588(20) keV [19]. After the peak positions were determined, they were fed into the detector simulation software GEANT4 [20], and the resultant response curves plus smooth polynomial backgrounds were used to analyze the experimental spectra and determine the cross sections at $\sigma^{\text{Pb}}(0_{\text{g.s.}}^+ \rightarrow 2_1^+) = 35 \pm 8$ and $\sigma^{pp}(0_{\text{g.s.}}^+ \rightarrow 2_1^+) = 24 \pm 4$ mb for the Pb and the liquid hydrogen target runs, respectively. For the cross section deduction, we used a procedure well tried in our earlier publications [4,6,21]; i.e., the number of incident particles were counted downstream of the target by setting the same gates which were used to produce the γ-ray spectra and exploiting that the ^{20}C and ^{19}C events were distinct in the TOF spectrum.

The results were phenomenologically analyzed in the framework of the coupled channels code ECIS97 [22], which uses standard collective form factors to calculate the inelastic cross sections. The procedure is detailed in Ref. [23]. In this way, the neutron and proton deformation lengths were extracted at $\delta_n = 1.57 \pm 0.14$ (stat), $\delta_p = 0.60 \pm 0.32$ (stat) fm. The corresponding reduced electric quadrupole transition probability $B(E2)$ and the multipole proton and neutron transition matrix elements M_p, M_n could then be calculated with the following formulas ($R = 1.2A^{1/3}$) [24–26]:

$$B(E2; 0_{\text{g.s.}}^+ \rightarrow 2_1^+)/e^2 = M_p^2 = \left(\frac{3}{4\pi} Z \delta_p R\right)^2, \quad (1)$$

$$M_n^2 = \left(\frac{3}{4\pi} N \delta_n R\right)^2, \quad (2)$$

as $M_p^2 = 7.8^{+10.6}_{-6.1}$(stat) and $M_n^2 = 292 \pm 52$ (stat) fm^4, respectively.

In these distorted wave calculations, the optical model parameters (OMP) were taken from a previous measurement of the ^{17}O+^{208}Pb reaction [27] for the Pb target run, while the global phenomenological parameter set $CH89$ proposed in Ref. [28] was used for the liquid hydrogen run. As was discussed in several earlier papers, e.g., Refs. [4,6,21,29], the uncertainty due to the choice of the optical potentials can be reliably tested by other sets of parameters. By independently switching from $CH89$ to Becchetti-Greenlees [30] parametrization and from the OMP of the ^{17}O+^{208}Pb reaction to that of the ^{12}C+^{208}Pb [31], the following total systematic errors were observed: $\Delta\delta_n = 0.015$, $\Delta\delta_p = 0.12$ fm; $\Delta M_n^2 = 6$, $\Delta M_p^2 = 3.4$ fm^4. On the other hand, the sensitivity parameters of the probes are not precisely known, which causes additional systematic uncertainty. This was tested by introducing a 20% change in the $(\frac{b_n}{b_p})^{pp}$ ratio

directly connected to the $(\frac{b_n}{b_p})^{\mathrm{Pb}}$ value, which resulted in the systematic errors $\Delta\delta_n = 0.04$, $\Delta\delta_p = 0.06$ fm; $\Delta M_n^2 = 15$, $\Delta M_p^2 = 1.7$ fm^4. Compared to these uncertainties, other sources of systematic errors (e.g., DALI2 efficiency and target thickness) were negligible.

In the above phenomenological analysis, we assumed an even contribution of neutrons and protons of the Pb probe when deducing the sensitivity parameters. However, a neutron skin exists at the surface of this probe where the reaction occurs, therefore the validity of the phenomenological approach was further examined by microscopic coupled-channels (MCC) calculations using folding model interactions with AMD transition density [32,33]. For the liquid hydrogen target, the folding model with the JLM interaction [34] was applied and resulted in $\sigma_{\mathrm{MCC}}^{pp} = 25.8$ mb coinciding with the experimental cross section (24 ± 4 mb). We adopted the standard values for the renormalization factors $(\lambda_R, \lambda_I) = (1.0, 0.8)$ and the range parameters $(t_R, t_I) = (1.2, 1.75)$ (fm) because the calculated results are found to be insensitive to them. For the Pb target, we used the double-folding model with the DDM3Y interaction for the real part of the potentials, and we introduced the imaginary potentials with the same geometrical form as the real ones having a renormalization factor, N_I, which is the only parameter of the calculation [35]. By changing its value from $N_I = 1.0$ to 1.4, only a small dependence was found on the calculated cross section, $\sigma_{\mathrm{MCC}}^{\mathrm{Pb}} = 41.8$–$39.5$ mb, which is consistent with the experimental value (35 ± 8 mb). The AMD transition density gives $M_p^2 = 24.62$ fm^4, which is very close to the upper limit of the experimental data, while the MCC calculations also provide the neutron strength of $M_n^2 = 250$ fm^4, consistent with the results of the phenomenological analysis.

The systematics of the M_p^2 and M_n^2 data for carbon isotopes are shown in Fig. 2, together with a global fit by Raman [26] which is based on the Grodzins rule [36]. The proton and neutron strengths are well correlated and follow the global trend up to $N = 14$. Above this point, however, their courses change; M_p^2 stays basically constant, while M_n^2 increases quickly with increasing neutron number and becomes an order of magnitude larger than the $B(E2)$ value in ^{20}C. Furthermore, M_n^2 is several times larger than the transition strength estimated from the transition energy by the Grodzins rule. This is associated with the large neutron excess. As seen in Eqs. (1) and (2), $B(E2)$ depends on Z^2, while M_n^2 on N^2. Thus, in a nucleus of large neutron excess such as ^{20}C, this results in a factor of about 5 enhancement of M_n^2 relative to $B(E2)$. Renormalizing M_n^2 by $(N/Z)^2$, the enhancement over the Grodzins rule can be eliminated, but the suppression of the $B(E2)$ relative to both the Grodzins rule and M_n^2 persists. This large difference between the neutron and proton transition probabilities can be interpreted as a signature of reduced polarization (and effective) charges in the carbon isotopes.

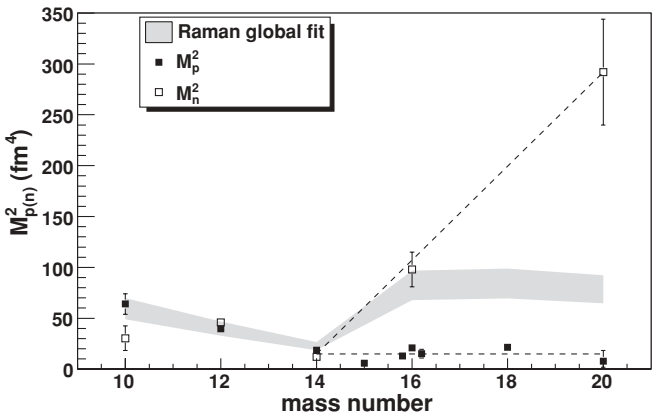

FIG. 2. Experimental M_p^2 and M_n^2 values and their statistical errors as a function of the mass number of carbon isotopes. The gray region represents a global fit plotted with its uncertainty by Raman [26] based on the Grodzins rule [36]. For ^{10,12,14,16,18}C isotopes, measured values are taken from Refs. [12,23,26,37–39]. The dashed lines are to guide the eye and reflect that M_p^2 practically becomes constant and M_n^2 shows a linear increase above $N = 14$.

To analyze the effective charges, the transition probabilities were calculated within the shell model. The wave functions and multiparticle $E2$ amplitudes were obtained in a model space of p shell for protons and sd shell for neutrons with the WBP interaction [40]. The $E2$ matrix elements were determined by combining the multiparticle amplitudes with the single-particle $E2$ matrix elements derived with radial wave functions in a mean field using the SkX Skyrme interaction [41]. For the Skyrme calculation, the sd-shell neutron orbital energies were constrained to the values of the $(N, Z) \rightarrow (N-1, Z)$ separation energies. The experimental M_p^2 data are plotted in Fig. 3 together with the results of the shell model calculations with normal [42] and reduced effective charges for neutron-rich carbon and oxygen isotopes (for comparison). The line with normal effective charges fits quite well the experimental data for oxygen isotopes except for ^{18}O due to intruder (4p-2h) admixtures [43]. However, a factor of about 0.4 reduction of the normal polarization charges is needed to reproduce the experimental trend in carbon isotopes. Furthermore, the available experimental M_n^2 values of ^{16,20}C (98 ± 17 and 292 ± 52 fm^4) are very close to the shell model calculations with the reduced effective charges (139 and 260 fm^4). We also note that unlike in the C isotopes, the linear increase of M_n^2 breaks in the O isotopes because of the $N = 14$ subshell closure ($M_n^2 = 42.8 \pm 2.2$, 186 ± 10, 248 ± 63, and 75 ± 43 fm^4 for ^{16,18,20,22}O, respectively [21,39,44–47]). The fact that the polarization charges have decreased to less than half of the standard values indicates that the coupling of the valence neutrons to the core has become weaker, or in other terms, the valence neutrons have decoupled to some extent from the nuclear core.

A possible reason for these decreased polarization charges might be the extended valence neutron distribution. In weakly bound nuclei, a neutron skin may develop, the thickness of which is expected to be proportional to the difference of the proton and neutron separation energies [48], suggesting that the neutron distribution in the less-bound C isotopes is wider, in agreement with nuclear radii measurements [49]. Assigning the increase of the nuclear size relative to a ^{14}C core to the valence neutrons using the prescription of Hansen and Jonson [2], the radius of the valence neutron distribution of carbon isotopes is much larger than that of the core

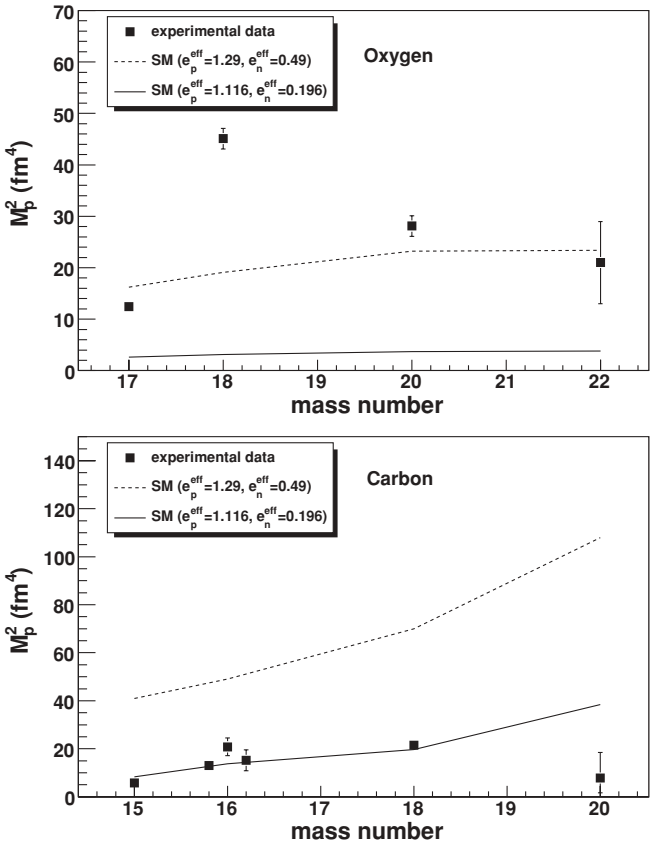

FIG. 3. Experimental M_p^2 values for neutron-rich oxygen and carbon isotopes and their statistical errors. The results of shell model calculations are drawn as dashed lines (normal effective charges) and solid lines (reduced effective charges). For the even nuclei, transitions are between 0^+ and 2^+; for the odd isotopes, they are between $5/2^+$ and $1/2^+$.

and that of the oxygen isotopes. This implies that for C nuclei, the valence neutrons spend more time outside of the core, resulting in a weaker polarization. The weakening of the interaction between the valence neutrons and the core protons and, as a consequence, the decrease of the polarization charges due to the extended neutron distribution have also been theoretically analyzed by Sagawa in a mean field approach [7]. His conclusion is also supported by a three-body calculation for ^{16}C [50].

Qualitatively, the polarization charges are inversely proportional to the radial matrix element of the orbit involved in the transition [43,51]. Comparing the reduction factors calculated with harmonic oscillator and Skyrme wave functions (which takes the relatively loose binding of the carbon isotopes into account), a ratio of $\approx$0.6 can be derived, which shows that the effects of weak binding qualitatively give the major part of the reduction. However, to fully understand this phenomenon, more detailed microscopic calculations giving a reliable radial distribution for weakly bound nuclei are necessary.

Summarizing our results, we have measured the cross section of the ^{1}H(^{20}C,^{20}C'γ) and ^{208}Pb(^{20}C,^{20}C'γ) processes and deduced the neutron and charge transition probabilities at $M_n^2 = 292 \pm 52$ (stat) fm^4 and $B(E2) < 18.4$ (stat) e^2 fm^4. The transition strengths have also been calculated in the *psd* shell model, and it was found that a suppression factor of 0.4 of both the proton and neutron polarization charges is needed to interpret the experimental results in carbon isotopes heavier than ^{14}C.

We thank the RIKEN Ring Cyclotron staff for their assistance during the experiment and Y. Kanada-En'yo for providing us with the AMD transiton densities for the ^{20}C nucleus. Z.E. is grateful for the Bolyai grant in Hungary. The European authors thank the kind hospitality and support from RIKEN. The present work was partly supported by the Grant-in-Aid for Scientific Research (No. 1520417) by the Ministry of Education, Culture, Sports, Science and Technology and by OTKA K68801, F60348, T049837, NKTH JP-16/2006, and by NSF Grant PHY-0758099.

[1] I. Tanihata *et al.*, Phys. Rev. Lett. **55**, 2676 (1985).
[2] P. G. Hansen *et al.*, Europhys. Lett. **4**, 409 (1987).
[3] H. Ogawa *et al.*, Phys. Rev. C **67**, 064308 (2003).
[4] Z. Dombrádi *et al.*, Phys. Lett. **B621**, 81 (2005).
[5] N. Imai *et al.*, Phys. Rev. Lett. **92**, 062501 (2004).
[6] Z. Elekes *et al.*, Phys. Lett. **B586**, 34 (2004).
[7] H. Sagawa and K. Asahi, Phys. Rev. C **63**, 064310 (2001).
[8] H. Sagawa *et al.*, Eur. Phys. J. A **13**, 87 (2002).
[9] Y. Suzuki *et al.*, Phys. Rev. C **70**, 051302(R) (2004).
[10] A. Ozawa *et al.*, Nucl. Phys. **A691**, 599 (2001).
[11] H. Sagawa, Phys. Rev. C **65**, 064314 (2002).
[12] M. Wiedeking *et al.*, Phys. Rev. Lett. **100**, 152501 (2008).
[13] D. Bazin *et al.*, Phys. Rev. Lett. **74**, 3569 (1995).
[14] F. M. Marques *et al.*, Phys. Lett. **B381**, 407 (1996).
[15] T. Baumann *et al.*, Phys. Lett. **B439**, 256 (1998).
[16] T. Kubo *et al.*, Nucl. Instrum. Methods B **70**, 309 (1992).
[17] H. Sakurai *et al.*, Phys. Lett. **B448**, 180 (1999).
[18] S. Takeuchi *et al.*, RIKEN Rev. **36**, 148 (2003).
[19] M. Stanoiu *et al.*, Phys. Rev. C **78**, 034315 (2008).
[20] S. Agostinelli *et al.*, Nucl. Instrum. Methods A **506**, 250 (2003).
[21] Z. Elekes *et al.*, Phys. Rev. C **74**, 017306 (2006).
[22] J. Raynal, Phys. Rev. C **23**, 2571 (1981).
[23] Z. Elekes *et al.*, Phys. Rev. C **78**, 027301 (2008).
[24] A. M. Bernstein, V. R. Brown, and V. A. Madsen, Phys. Rev. Lett. **42**, 425 (1979).
[25] A. M. Bernstein *et al.*, Phys. Lett. **B103**, 255 (1981).
[26] S. Raman *et al.*, At. Data Nucl. Data Tables **78**, 1 (2001).
[27] J. Barrette *et al.*, Phys. Lett. **B209**, 182 (1988).
[28] R. Varner *et al.*, Phys. Rep. **201**, 57 (1991).
[29] H. J. Ong *et al.*, Phys. Rev. C **73**, 024610 (2006).
[30] F. D. Becchetti *et al.*, Phys. Rev. **182**, 1190 (1969).
[31] C.-C. Sahm *et al.*, Phys. Rev. C **34**, 2165 (1986).
[32] Y. Kanada-En'yo, Phys. Rev. C **71**, 014310 (2005).
[33] Y. Kanada-En'yo (private communication).
[34] J. P. Jeukenne, A. Lejeune, and C. Mahaux, Phys. Rev. C **16**, 80 (1977).
[35] M. Takashina, Y. Kanada-Enyo, and Y. Sakuragi, Phys. Rev. C **71**, 054602 (2005).

[36] L. Grodzins, Phys. Lett. **2**, 88 (1962).
[37] H. J. Ong *et al*., Phys. Rev. C **78**, 014308 (2008).
[38] C. Jouanne *et al*., Phys. Rev. C **72**, 014308 (2005).
[39] R. J. Peterson, Phys. Rev. C **48**, 1128 (1993).
[40] E. K. Warburton and B. A. Brown, Phys. Rev. C **46**, 923 (1992).
[41] B. A. Brown, Phys. Rev. C **58**, 220 (1998).
[42] B. A. Brown *et al*., Annu. Rev. Nucl. Part. Sci. **38**, 29 (1988).
[43] B. A. Brown, Nucl. Phys. **A277**, 77 (1977).
[44] J. K. Jewell *et al*., Phys. Lett. **B454**, 181 (1999).
[45] D. T. Khoa, Phys. Rev. C **68**, 011601(R) (2003).
[46] E. Jewell *et al*., Phys. Lett. **B490**, 45 (2000).
[47] E. Becheva *et al*., Phys. Rev. Lett. **96**, 012501 (2006).
[48] T. Suzuki *et al*., Phys. Rev. Lett. **75**, 3241 (1995).
[49] A. Ozawa *et al*., Nucl. Phys. **A693**, 32 (2001).
[50] W. Horiuchi and B. A. Suzuki, Phys. Rev. C **73**, 037304 (2006).
[51] A. Bohr and B. R. Mottelson, *Nuclear Structure* (World Scientific, Singapore, 1998), Vol. 2 .